Supporting Information

High Rate Capability and Long Lifespan Symmetric Sodium-ion Battery System Based on Bipolar Material $Na_2LiV_2(PO_4)_3$/C

Meng Li [a], Zonglin Zuo [a], Jianqiu Deng [a, c], Qingrong Yao* [c], Zhongmin Wang [a, c], Huaiying Zhou [a, c], Wen-Bin Luo* [b], Hua-Kun Liu [b], Shi-Xue Dou[b]*

[a] School of Material Science and Engineering, Guilin University of Electronic Technology, Guangxi, Guilin 541004, China
E-mail: jqdeng@guet.edu.cn

[b] Institute for Superconducting and Electronic Materials, University of Wollongong, Squires Way, Fairy Meadow, NSW 2500, Australia
E-mail: luow@uow.edu.au

[c] Guangxi Key Laboratory of Information Materials, Guilin University of Electronic Technology, Guangxi, Guilin 541004, China

Keywords: Sodium-ion batteries; Bipolar materials; Symmetric full cell; $Na_2LiV_2(PO_4)_3$;

Nanocomposite

Experimental

Synthesis of active material : Nanosized $Na_2LiV_2(PO_4)_3$/C (NLVP/C) was synthesized via a sol-gel method using Na_2CO_3, $LiOH{\cdot}H_2O$, NH_4VO_3, $NH_4H_2PO_4$, oxalic acid, and glucose as starting materials. First, NH_4VO_3 and oxalic acid were dissolved in 50 mL of deionized water under magnetic stirring at 70 ^oC to form a clear orange solution. Then, stoichiometric amounts of Na_2CO_3, $LiOH{\cdot}H_2O$, $NH_4H_2PO_4$, and glucose were added to the solution, and the mixed solution was stirred continually until the green precursor gel was obtained. The amount of glucose was based on 10 wt.% residual carbon content of NLVP/C. Finally, the obtained gel was dried at 120 ^oC for 12 h in a vacuum oven. After grinding, the precursor was pre-heated at 350 ^oC for 4 h and calcined at 750 ^oC for 10 h in a tube furnace under flowing Ar containing 5% H_2 to yield the final product. The pure NLVP was also prepared according to the same synthetic route of NLVP/C except for the addition of glucose.

Materials characterizations: The crystalline phase of the product was characterized by X-ray diffraction (XRD) using a PIXcel^{3D} power diffractometer with Cu Kα radiation in the 2θ range of 10 – 80° at a scan rate of 2 °/min. The morphology and particle size of NLVP/C were observed with a scanning electron microscope (FESEM, HitachiS-4800) and a high-resolution transmission electron microscope (HRTEM, Tecnai G2 F20, 200 kV). The carbon content of NLVP/C was determined by thermogravimetric (TG) analysis. X-ray photoelectron spectroscopy (XPS) was carried out using an ESCALAB-250Xi spectrometer. Raman spectra were obtained from a LabRAM HR Evolution Raman micro-spectroscope with 532 nm laser radiation in the range of 100–2000 cm^{-1}.

Electrochemical measurements: The electrochemical performance of NLVP/C was measured by using 2023-type coin cell. The working electrodes was prepared by milling a mixture of 70 wt% active material, 20 wt% Super P carbon, and 10 wt% polyvinylidene fluoride (PVDF) in N-methyl-2-pyrrolidone (NMP). The obtained slurry was spread onto aluminum foil and dried

at 120 °C for 12 h in a vacuum oven. The electrode loading mass is around 1.5 to 2.0 mg cm^{-2}. After punching the electrode film into disks with the diameters of 1.4 cm (cathode) and 1.2 cm (anode), the cells were assembled in an argon-filled glove box using NLVP/C as cathode, sodium metal as anode, Whatman glass fiber (Grade GF/D) as separator, and a 1 M solution of $NaClO_4$ in ethylene carbonate (EC) and diethyl carbonate (DEC) (1:1 by volume) as the electrolyte. Full sodium ion cells were constructed using NLVP/C as cathode and anode. The mass ratio of the cathode and anode was designed to be close to 2:1. All the cells were tested at room temperature. The galvanostatic charge–discharge cycling was performed on an Arbin BT2000 automatic battery testing system. The electrochemical impedance spectroscopy (EIS) and cyclic voltammetry (CV) were carried out on a Solartron electrochemical workstation. The chemical diffusion coefficients of Na ions in the electrodes can be calculated using Fick's second law by Equation (1) [48]:

$$D_{Na^+} = \frac{4}{\pi}\left(\frac{m_B V_M}{M_B A}\right)\left(\frac{\Delta E_s}{\tau \, dE_\tau / d\sqrt{\tau}}\right)^2 \quad (\tau << L^2/D_{Na^+}) \qquad (1)$$

In this equation, V_M is the molar volume of the active materials, M_B and m_B are the molecular weight (g mol^{-1}) and mass loading (g) of the active materials (sodium host). A is the surface area of the electrode, L is the thickness of the electrode, τ is the titration time, and ΔE_s is the difference between the original voltage E_0 and the steady-state voltage E_s (**Figure S6a**, Supporting Information). The value of $dE_\tau/d\tau^{1/2}$ can be obtained from a plot of the voltage versus the square root of the time during the current pulse. When the voltage shows a linear relationship with $\tau^{1/2}$ during titration, as in **Figure S6b** , Eq. (2) can be simplified as [48]:

$$D_{Na^+} = \frac{4}{\pi\tau}\left(\frac{m_B V_M}{M_B A}\right)\left(\frac{\Delta E_s}{\Delta E_\tau}\right)^2 \qquad (2)$$

Table S1. Atomic positions of (a) rhombohedral $Li_3V_2(PO_4)_3$ and (b) rhombohedral $Na_3V_2(PO_4)_3$ deduced from the Rietveld refinement of XRD data.

(a)

Atom	Wyckoff site	*x*	*y*	*z*
V1	18	0	0	0.14615
V2	18	0	0	0.65310
P1	18	0.29233	0.00187	0.25136
O1	18	0.19148	-0.00958	0.19192
O2	18	0.76561	0.91258	0.68983
O3	18	0.24341	0.80073	0.26840
O4	18	0.50057	0.87958	0.75564
Li1	18	0.34105	0.02406	0.38187

(b)

Atom	Wyckoff site	*x*	*y*	*z*
Na1	36	0	0	0
Na2	36	0.63481	0	0.25002
V1	36	0	0	0.14876
P1	36	0.29026	0	0.25005
O1	36	0.17933	-0.02673	0.19371
O2	36	0.19111	0.16856	0.08895

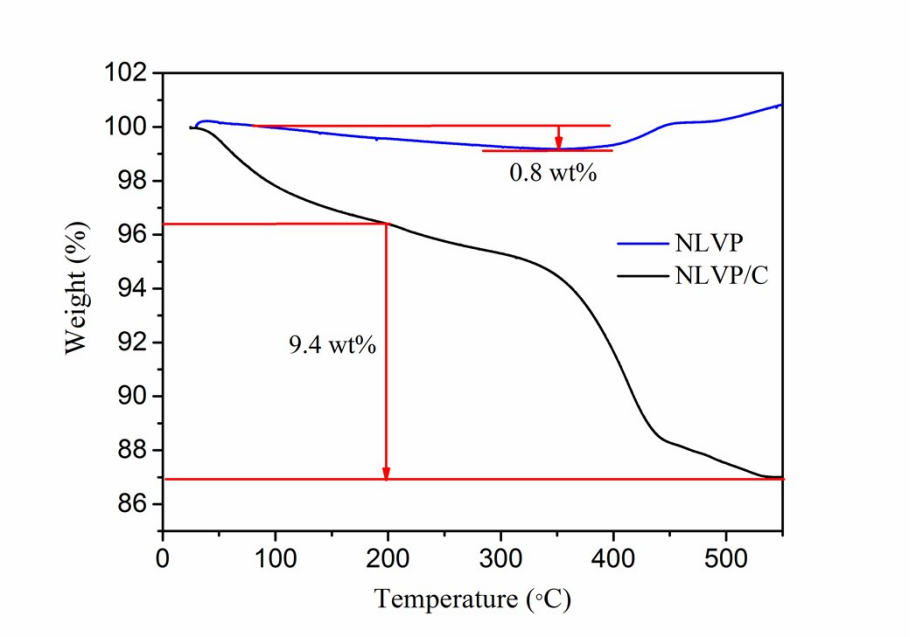

Figure S1. TGA curve of pure NLVP and NLVP/C.

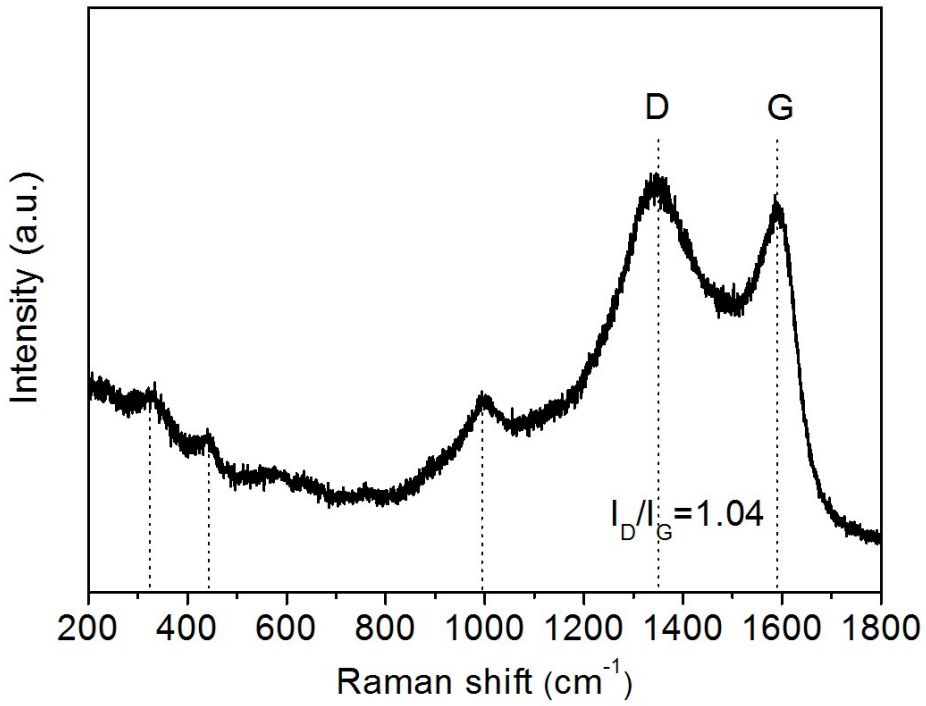

Figure S2. Raman spectrum of NLVP/C.

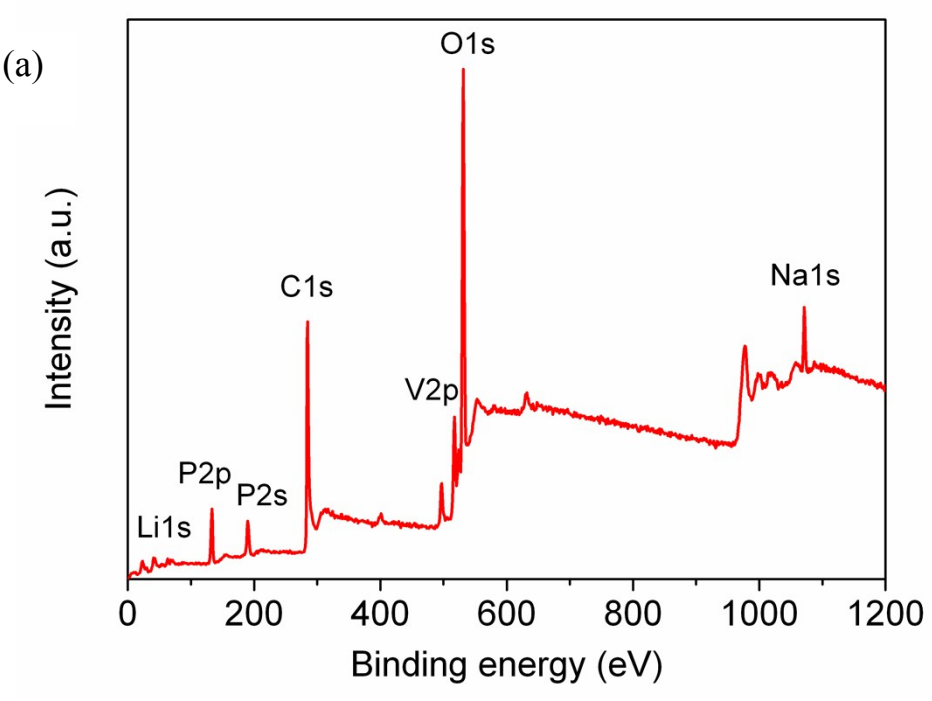
(a)
O1s
C1s
Na1s
V2p
P2p
P2s
Li1s
Intensity (a.u.)
0
200
400
600
800
1000
1200
Binding energy (eV)

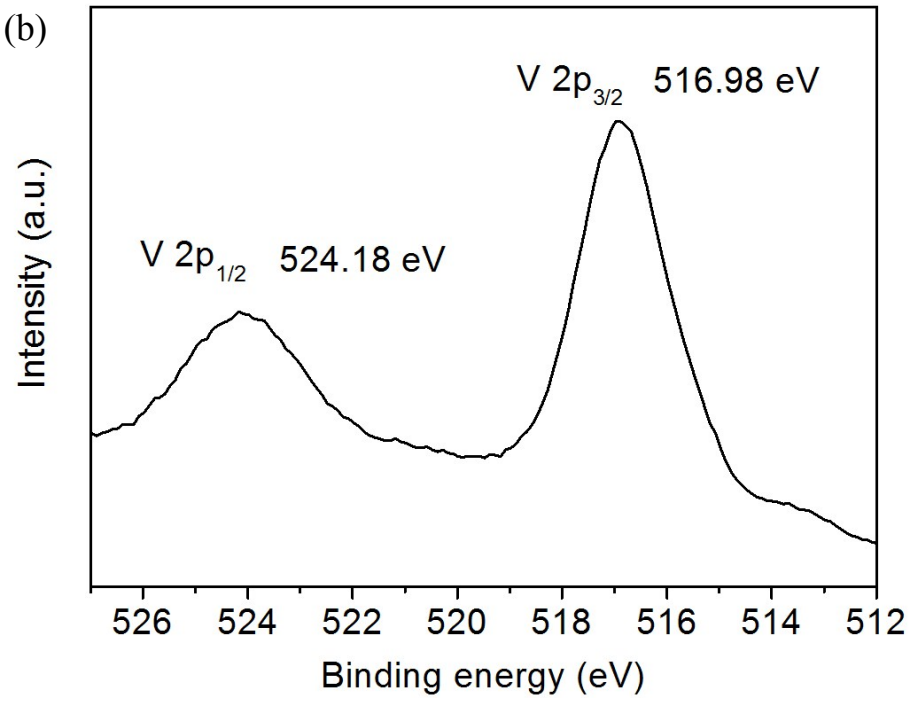
(b)
V 2p3/2 516.98 eV
V 2p1/2 524.18 eV
Intensity (a.u.)
526
524
522
520
518
516
514
512
Binding energy (eV)

(c)

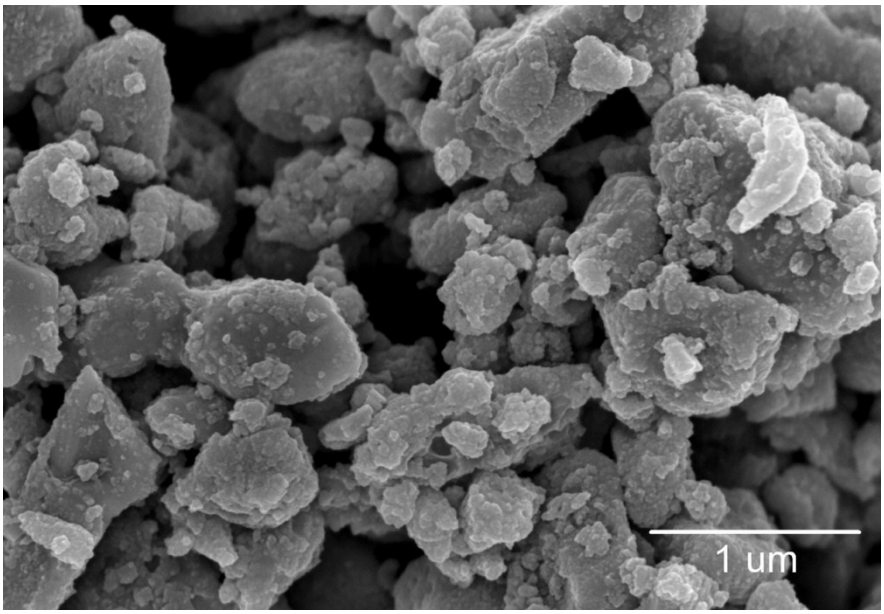

(d)

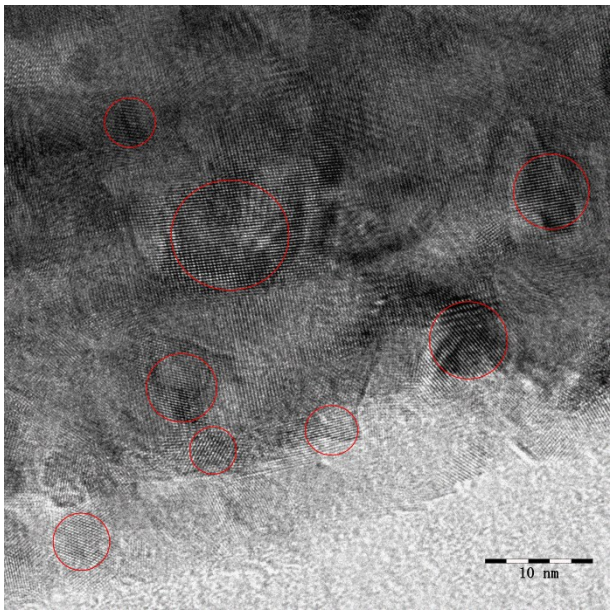

Figure S3. (a, b) XPS spectra, (c) SEM image and (d) HRTEM image of NLVP/C.

(a)

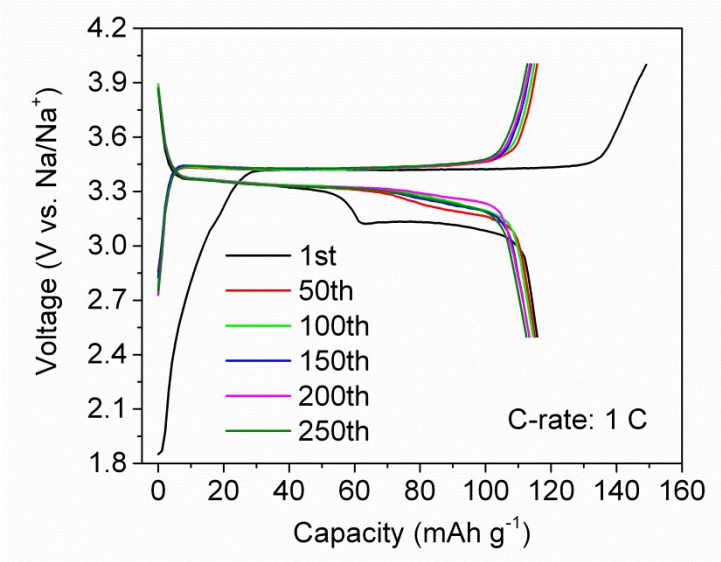
Voltage (V vs. Na/Na+)
Capacity (mAh g-1)
1st
50th
100th
150th
200th
250th
C-rate: 1 C

(b)

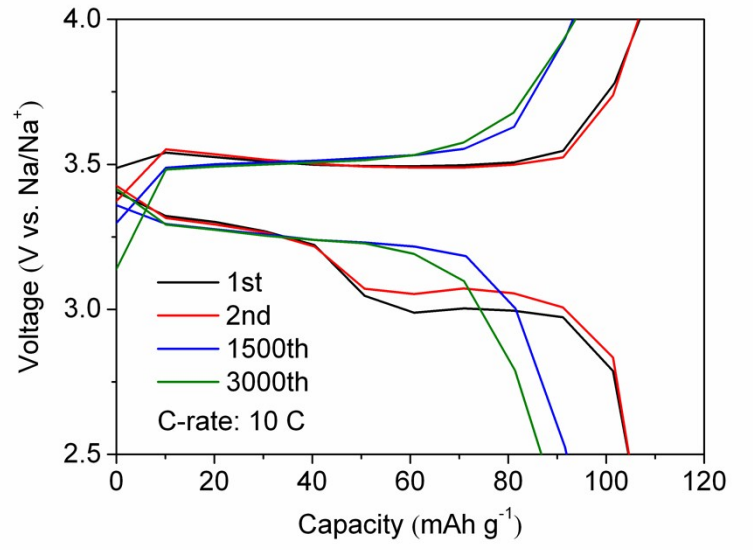
Voltage (V vs. Na/Na+)
Capacity (mAh g-1)
1st
2nd
1500th
3000th
C-rate: 10 C

(c)

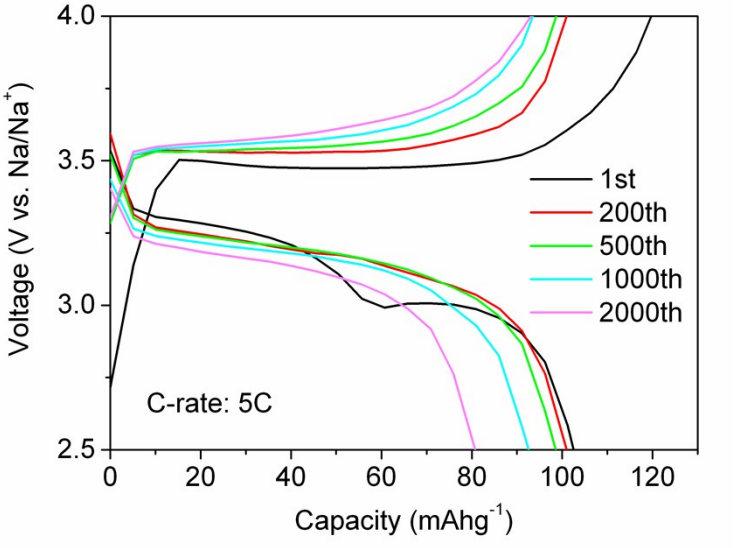
Voltage (V vs. Na/Na+)
Capacity (mAhg-1)
1st
200th
500th
1000th
2000th
C-rate: 5C

(d)

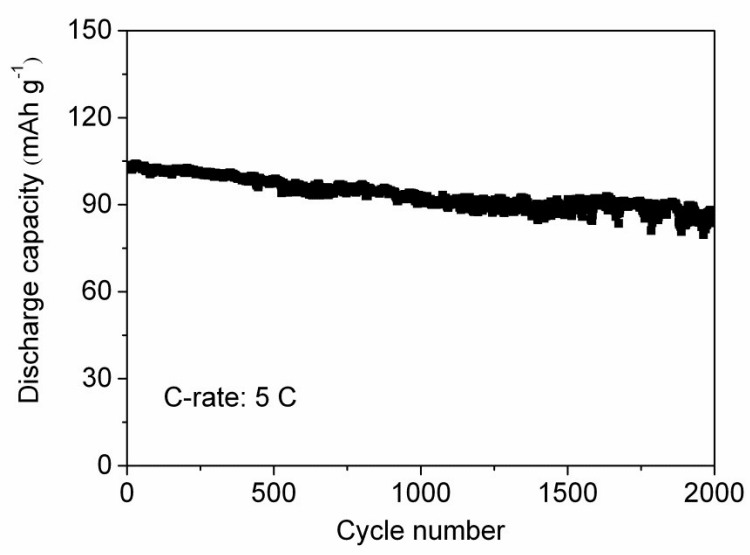

Figure S4. Charge and discharge curves of NLVP/C as cathode material at 1 C (a), 10 C (b), and 5 C (c); (d) Cycling performance of NLVP/C at 5 C.

Table S2. Comparison of electrochemical properties of NLVP/C in this work with those of various previously reported polyanion-type cathodes for SIBs.

Cathodes	Reversible capacity	Capacity retention	Ref.
$Na_3V_2(PO_4)_3$@C nanocomposite	94.9 mAh g^{-1}, 5 C	96.1%, 5 C, 700 cycles	S1
$Na_3V_2(PO_4)_3$/C particles	107.6 mAh g^{-1}, 1 C 106.3 mAh g^{-1}, 2 C 95.6 mAh g^{-1}, 5 C	74.4%, 1 C, 600 cycles 63.0%, 2 C, 200 cycles 60.7%, 5 C, 200 cycles	S2
$Na_3V_2(PO_4)_3$@C@CMK-3	109 mAh g^{-1}, 5 C 106 mA h g^{-1}, 10 C 102 mAh g^{-1}, 20 C	68%, 5 C, 2000 cycles 85%, 10 C, 1000 cycles 67.3%, 20 C, 1000 cycles	S3
$Na_3V_2(PO_4)_3$/C+N particles	104.6 mAh g^{-1}, 1 C 74.5 mAh g^{-1}, 5 C	86.8%, 1 C, 100 cycles 92.6%, 5 C, 100 cycles	S4
$NaFePO_4$/C	99.4 mAh g^{-1}, 0.5 C	95%, 0.5 C, 200 cycles	S5
$Na_7V_4(P_2O_7)_4(PO_4)$/C nanorod	92.1 mAh g^{-1}, 0.05 C	95.2%, 0.05 C, 200 cycles 92.6%, 0.5 C, 200 cycles	S6
Ultrafine $Na_7V_3(P_2O_7)_4$/C	73 mAh g^{-1}, 0.025 C	92%, 10 C, 100 cycles	S7
$Na_{3.32}Fe_{2.34}(P_2O_7)_2$@C	72.5 mAh g^{-1}, 5 C	90%, 5 C, 1100 cycles	S8
$Na_3V_2(PO_4)_2F_3$/C@RGO	124.5 mAh g-1, 1 C	87%, 1 C, 700 cycles	S9
CNT-decorated $Na_3V_2(PO_4)_3$ microspheres	96.0 mAhg-1, 10 C	92.60%, 10 C, 150 cycles	S10
$NaVPO_4F$/C Nanofibers	100 mAh g^{-1}, 2 C	96.5%, 2C, 1000 cycles	S11
Na_2FePO_4F-rGO composites	60 mAh g^{-1}, 10 C	70%, 10C, 5000 cycles	S12
$Na_3V_2O_2(PO_4)_2F$/rGO microsphere composite	90 mAh g^{-1}, 30 C	83.4%, 30 C, 2000 cycles	S13
$Na_2LiV_2(PO_4)_3$/C nanocomposite	115.8 mAh g^{-1}, 1 C 104.8 mAh g^{-1}, 10 C	97.2%, 1 C, 250 cycles 83%, 10 C, 3000 cycles	This work

(a)

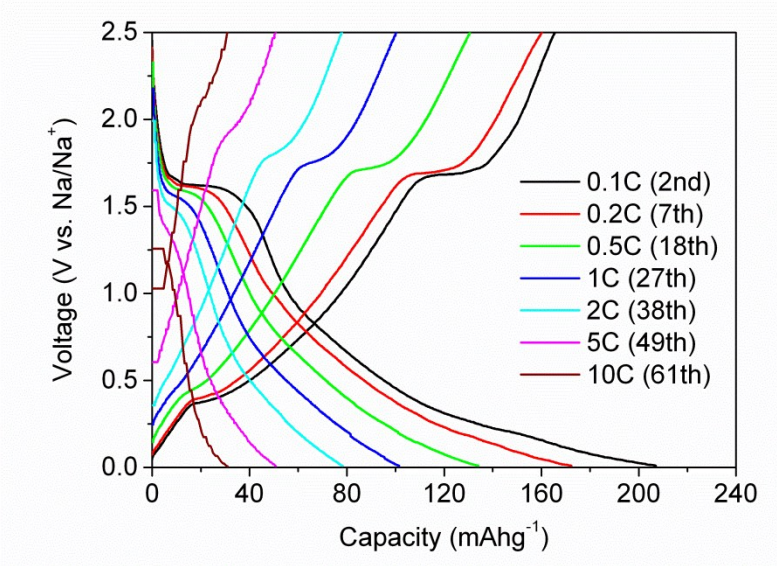
Voltage (V vs. Na/Na+)
Capacity (mAhg-1)
0.1C (2nd)
0.2C (7th)
0.5C (18th)
1C (27th)
2C (38th)
5C (49th)
10C (61th)

(b)

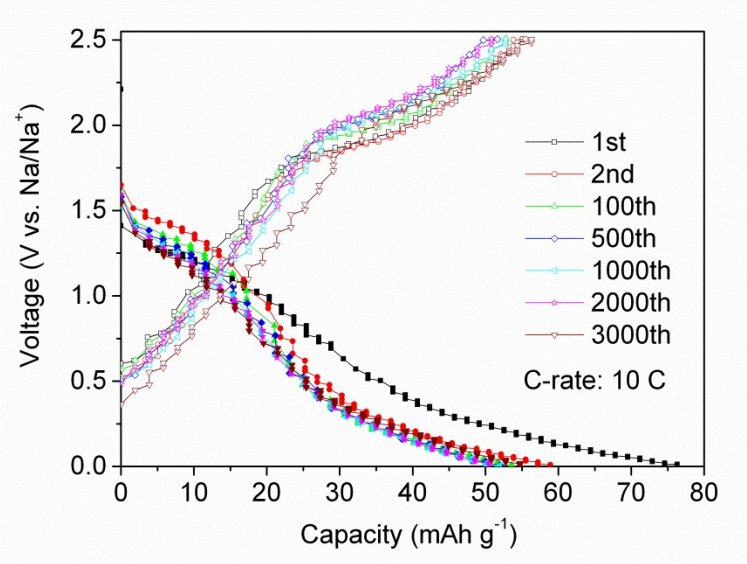
Voltage (V vs. Na/Na+)
Capacity (mAh g-1)
1st
2nd
100th
500th
1000th
2000th
3000th
C-rate: 10 C

(c)

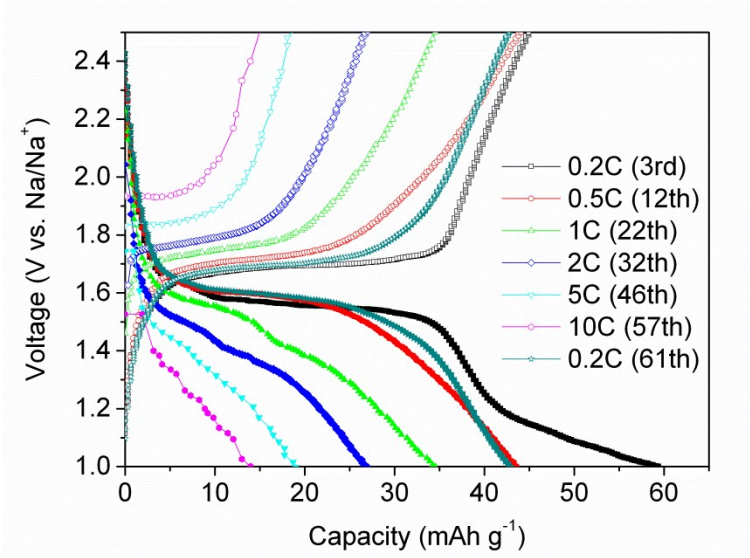
Voltage (V vs. Na/Na+)
Capacity (mAh g-1)
0.2C (3rd)
0.5C (12th)
1C (22th)
2C (32th)
5C (46th)
10C (57th)
0.2C (61th)

(d)

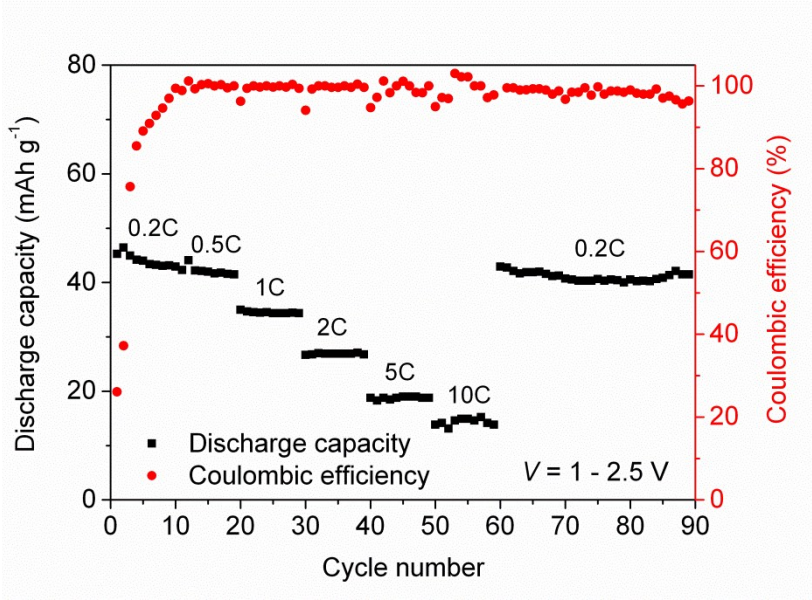
Discharge capacity (mAh g-1)
Coulombic efficiency (%)
Cycle number
0.2C
0.5C
1C
2C
5C
10C
0.2C
Discharge capacity
Coulombic efficiency
V = 1 - 2.5 V

(e)

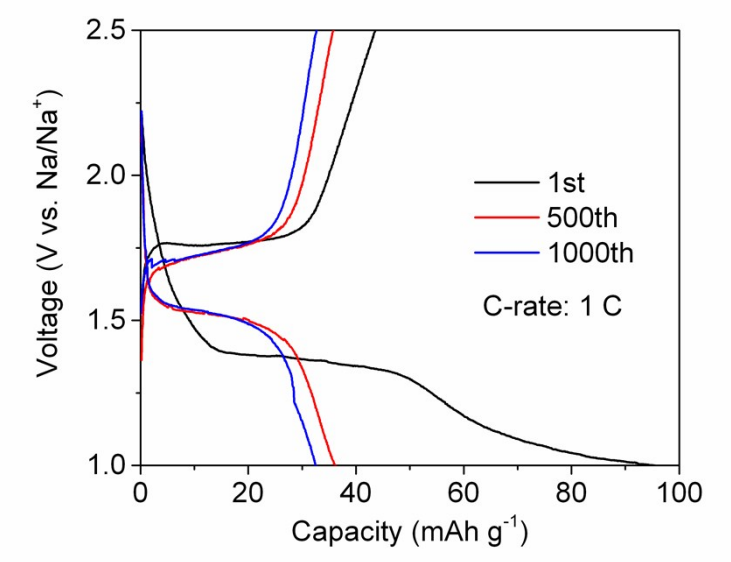

(f)

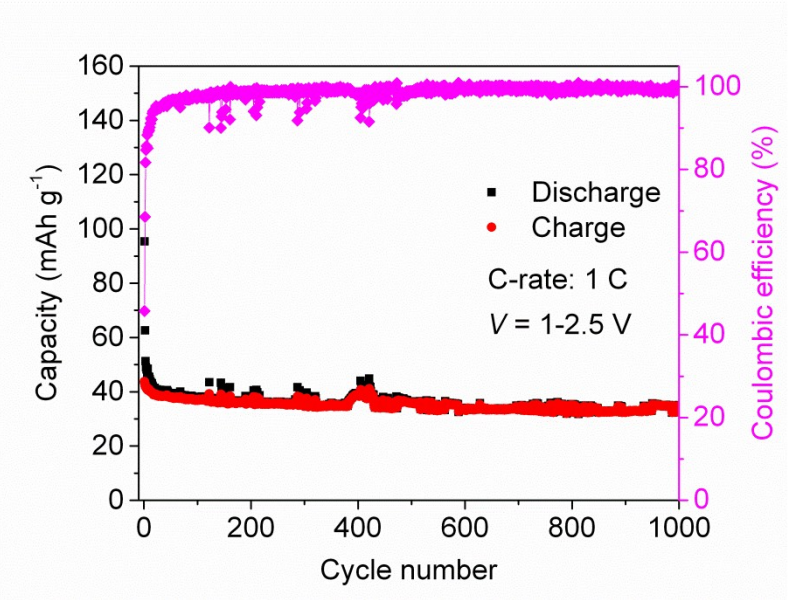

Figure S5. (a) Discharge/charge curves of NLVP/C as anode at different current rates. (b) Discharge/charge curves of NLVP/C at 10 C. (c) Discharge/charge curves and (d) rate capability of NLVP/C as anode at different current rates. (e, f) Discharge/charge curves and cycling performance of NLVP/C at 1 C. The voltage window was 1.0−2.5 V for all these measurements.

(a)

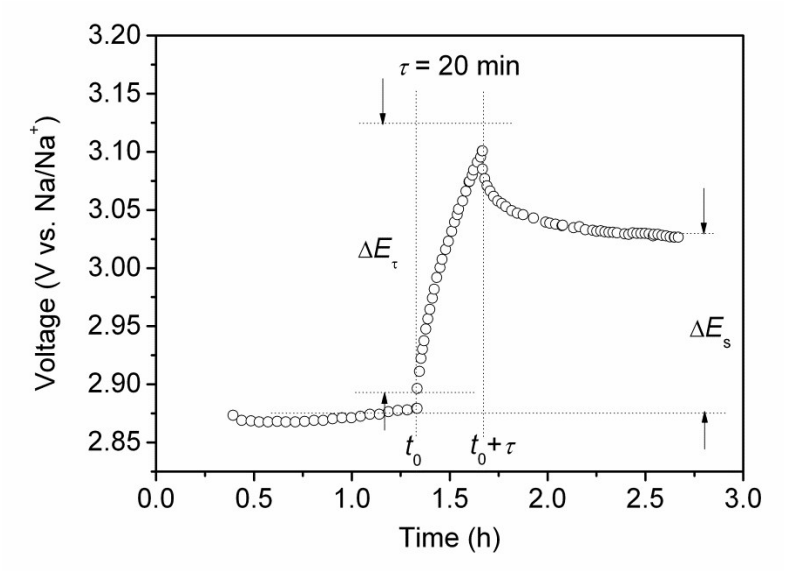
τ = 20 min
ΔE_τ
ΔE_s
t_0
t_0+τ
Voltage (V vs. Na/Na+)
Time (h)
3.20
3.15
3.10
3.05
3.00
2.95
2.90
2.85
0.0
0.5
1.0
1.5
2.0
2.5
3.0

(b)

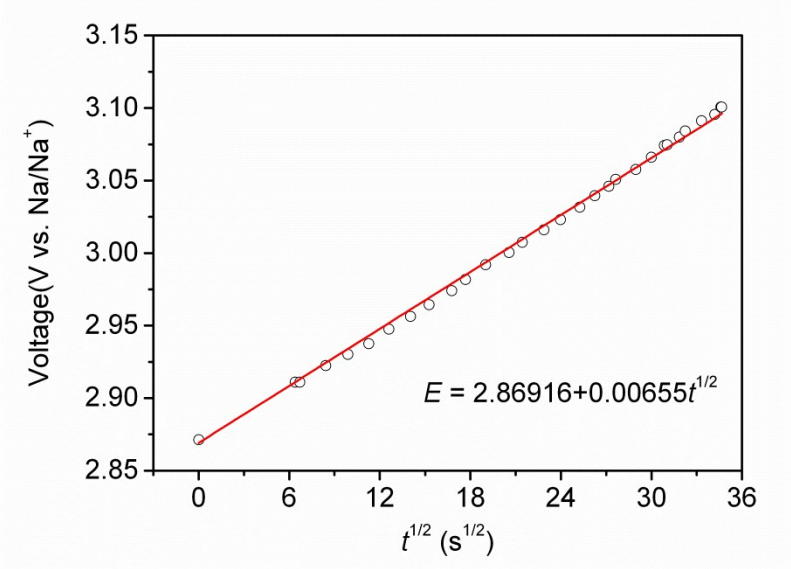
E = 2.86916+0.00655t^1/2
Voltage(V vs. Na/Na+)
t^1/2 (s^1/2)
3.15
3.10
3.05
3.00
2.95
2.90
2.85
0
6
12
18
24
30
36

(c)

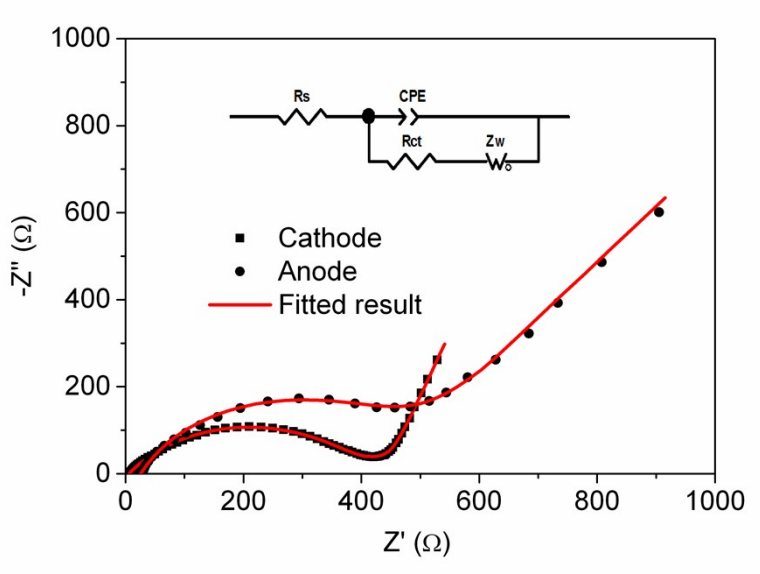

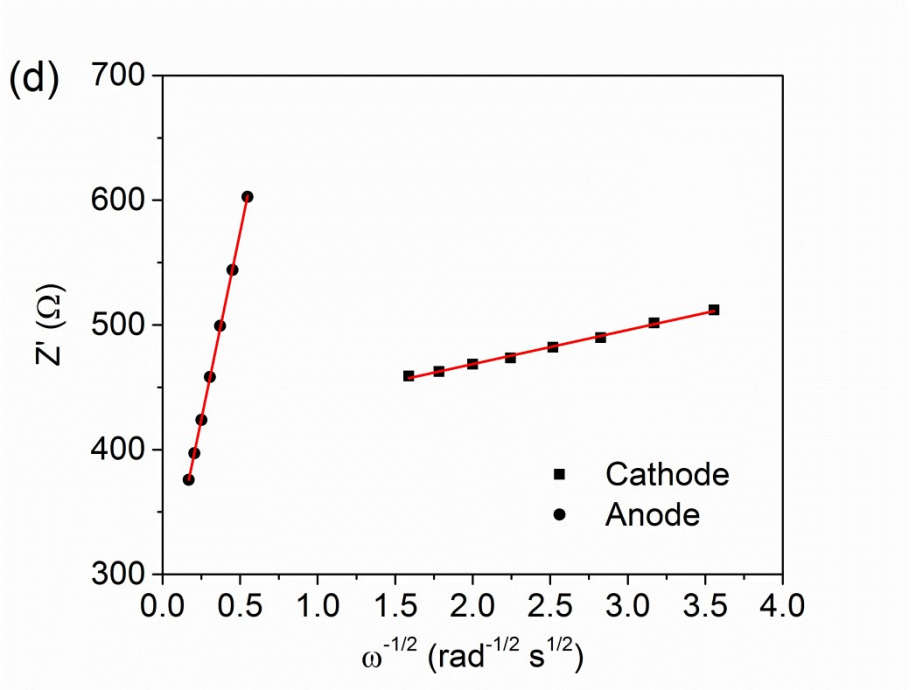

Figure S6. (a) Demonstration of a single titration at 2.88V during the GITT test of NLVP/C cathode. (b) Plot of the linear relationship of voltage against $\tau^{1/2}$ during a single titration at 2.88 V. (c) Nyquist plots and fitting curves of NLVP/C electrodes after 10 charge–discharge cycles. (d) The relationship between Z′ and $\omega^{-1/2}$ at low frequency region for NLVP/C electrodes.

(a)

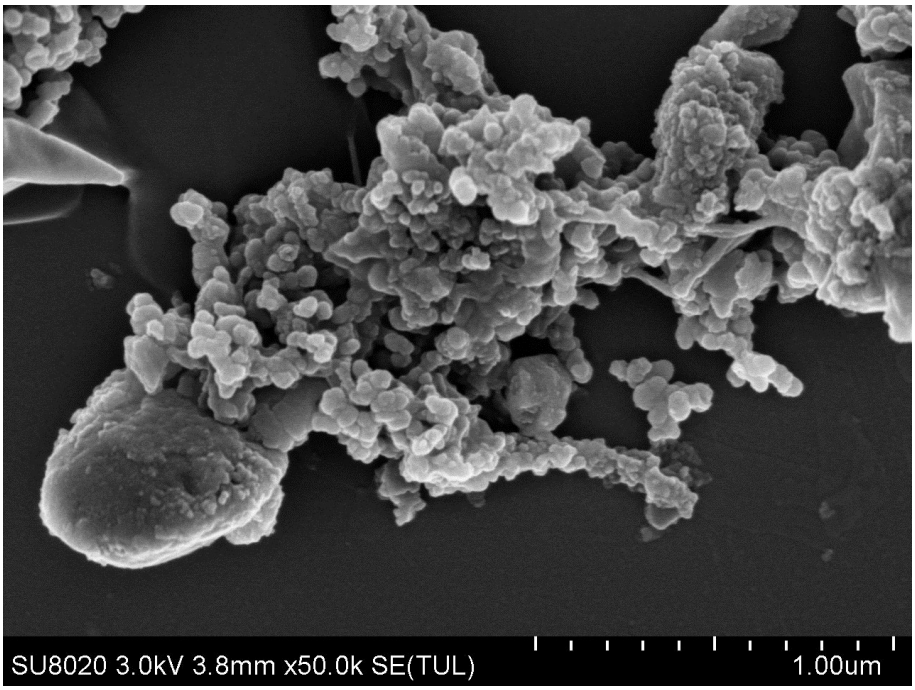

(b)

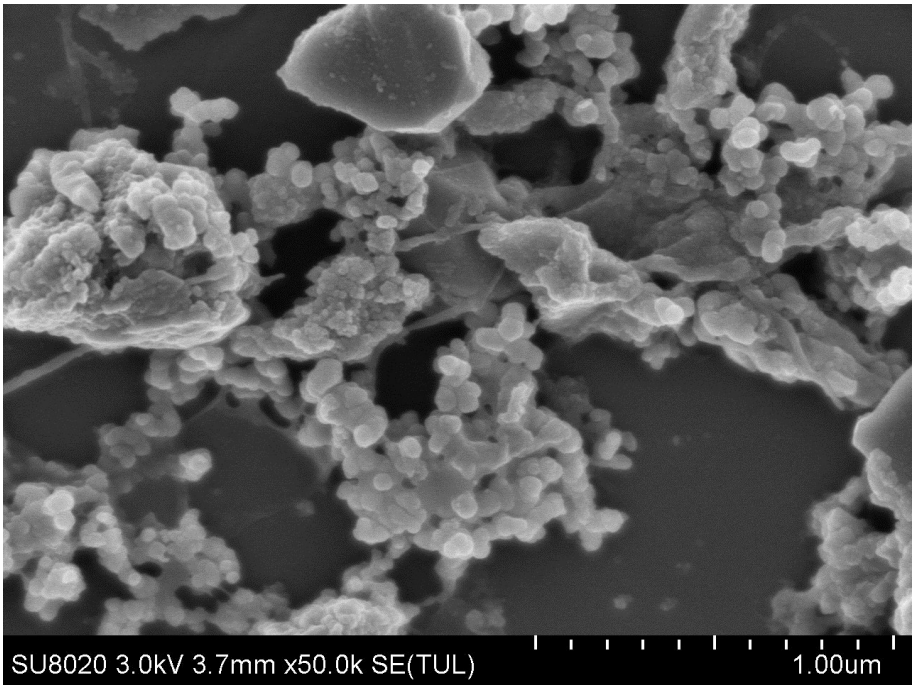

Figure S7. SEM images of (a) the as-prepared electrode and (b) the cycled electrode over 250 cycles at 1 C.

References:

[S1] W. Duan, Z. Zhu, H. Li, Z. Hu, K. Zhang, F. Cheng and J. Chen, *J. Mater. Chem. A*, 2014, **2**, 8668–8675.

[S2] H. Li, X. Bi, Y. Bai, Y. Yuan, R. Shahbazian-Yassar, C. Wu, F. Wu, J. Lu and K. Amine, *Adv. Mater. Interfaces*, 2016, **3**, 1500740.

[S3] Y. Jiang, Z. Yang, W. Li, L. Zeng, F. Pan, M. Wang, X. Wei, G. Hu, L. Gu and Y. Yu, *Adv. Energy Mater.*, 2015, **5**, 1402104.

[S4] W. Shen, C. Wang, Q. Xu, H. Liu and Y. Wang, *Adv. Energy Mater.*, 2014, **5**, 1400982.

[S5] J. Kim, D.-H. Seo, H. Kim, I. Park, J.-K. Yoo, S.-K. Jung, Y.-U. Park, W. A. Goddard III, and K. Kang, *Energy Environ. Sci.*, 2015, **8**, 540–545.

[S6] C. Deng and S. Zhang, *ACS Appl. Mater. Interfaces*, 2014, **6**, 9111–9117.

[S7] C. Deng, S. Zhang and B. Zhao, *Energy Storage Mater.* 2016, **4**, 71–78.

[S8] M. Chen, L. Chen, Z. Hu, Q. Liu, B. Zhang, Y. Hu, Q. Gu, J.-L. Wang, L.-Z. Wang, X. Guo, S.-L. Chou and S.-X. Dou, *Adv. Mater.* 2017, **29**, 1605535.

[S9] L. Li, Y. Xu, X. Sun, S. He and L. Li, *Chem. Eng. J.*, 2018, **331**, 712–719.

[S10] H. Chen, B. Zhang, X. Wang, P. Dong, H. Tong, J.-C. Zheng, W. Yu and J. Zhang, *ACS Appl. Mater. Interfaces,* 2018, **10**, 3590−3595.

[S11] T. Jin, Y. Liu, Y. Li, K. Cao, X. Wang and L. Jiao, *Adv. Energy Mater.*, 2017, **7**, 1700087.

[S12] J.S. Ko, V.V.T. Doan-Nguyen, H.-S. Kim, X. Petrissans, R.H. DeBlock, C.S. Choi, J.W. Long and B.S. Dunn, *J. Mater. Chem. A*, 2017, **5**, 18707–18715.

[S13] Y. Yin, F. Xiong, C. Pei, Y. Xu, Q. An, S. Tan, Z. Zhuang, J. Sheng, Q. Li and L. Mai, Nano Energy, 2017, **41**, 452–459.